RSC Advances

PAPER

View Article Online
View Journal | View Issue

Cite this: *RSC Adv.*, 2019, **9**, 2172

Al_2O_3-coated $Li_{1.2}Mn_{0.54}Ni_{0.13}Co_{0.13}O_2$ nanotubes as cathode materials for high-performance lithium-ion batteries

Yangwen Chen,[ab] Xinchang Wang,[*a] Jiajia Zhang,[ab] Baiyuan Chen,[c] Junmin Xu,[a] Sen Zhang[a] and Liwei Zhang[*b]

Received 15th November 2018
Accepted 8th January 2019

DOI: 10.1039/c8ra09428d

rsc.li/rsc-advances

Li-rich manganese-based layered cathode $Li_{1.2}Mn_{0.54}Ni_{0.13}Co_{0.13}O_2$ (LMNCO) nanotubes are synthesized by electrospinning and surface coated with different amounts of amorphous Al_2O_3. The effects of the coating content of Al_2O_3 on the structural and electrochemical performances of LMNCO nanotubes are investigated systematically. The results show that the morphologies and structures of the samples exhibit no apparent changes after being coated with Al_2O_3. Electrochemical tests indicate that the Al_2O_3-coated LMNCO nanotubes exhibit obviously enhanced electrochemical performances. The initial coulombic efficiency of surface modified LMNCO nanotubes increased from 74.9% to 85.2%, and the modified LMNCO nanotubes have a high capacity retention of 97.6% after 90 cycles at 1C. The improved electrochemical performances of the coated samples are attributed to the protective function of the uniform Al_2O_3 coating and the three-dimensional Li^+ diffusion channel in the spinel interface layer.

1. Introduction

Lithium-ion batteries (LIBs) have become one of the most important power battery options, and have excellent application prospects in the fields of portable electronic products and electric vehicles (EVs).[1,2] Cathode materials, as key performance limiting factors for battery energy and power density, have been vigorously researched in recent years. In this context, the Layered Li-rich Manganese Oxides (LLOs), with a chemical formula $(xLi_2MnO_3 \cdot (1-x)LiMO_2$, M = Mn, Co, Ni…), have attracted more and more attention because of their lower cost and higher energy density.[3–5] The specific capacity and average discharge voltage of layered lithium-rich manganese oxides are about 250–300 mA h g^{-1} and 3.5 V, and the energy density can reach 900 W h kg^{-1}, which is almost twice that of the common cathode materials like $LiFePO_4$, $LiCoO_2$ and $LiMn_2O_4$.[6,7] However, there are also several problems that seriously limit their commercial application. For example, severe irreversible capacity loss in the first cycle is ascribed to the release of lithium and oxygen at high potentials during the first charge process.[8] What is more, the side reactions occurring at the electrolyte/electrode interface at high voltages will result in general capacity retention. In addition, low Li^+ diffusion coefficient and electronic conductivity of layered lithium-rich manganese oxides lead to poor rate capability.[9–12]

One-dimensional (1D) nanostructure materials prepared by electrospinning have attracted more and more attention, because this kind of nanostructure not only has short ionic diffusion pathways and electron transport paths, but also provides more contact areas between electrolytes and electrode materials.[13] Xu *et al.* prepared $Li_{1.2}Mn_{0.54}Ni_{0.13}Co_{0.13}O_2$ nanofibers and nanoparticles by electrospinning method and coprecipitation method respectively. The initial coulombic efficiency of the nanofibers is 75%, which is higher than the 68.2% of the nanoparticles.[14] Ma *et al.* used electrospinning method to fabricate $Li_{1.2}Mn_{0.54}Ni_{0.13}Co_{0.13}O_2$ nanotubes, and the materials displayed an excellent cyclic and rate performance.[15] Cui *et al.* reported the effect of different calcination times on the electrochemical properties of LMNCO nanotubes, and found that the LMNCO materials calcined at 800 °C for 8 h had a capacity retention of 68.47% after 50 cycles.[16]

Surface coating materials have found an increasingly wide utilization in the field of lithium-ion batteries, such as $AlPO_4$,[17] Al_2O_3,[18] rGO,[19] MgO,[20] which can prevent the direct contact between the electrolytes and electrode materials, effectively decrease the side reaction occurring at the electrode/electrolyte interface. Zhou *et al.* used sol–gel method coating Al_2O_3 (5–20 nm) on the surface of LLOs, and the voltage fading during the cycle was effectively suppressed.[21] Atomic layer deposition has several outstanding advantages over conventional methods, such as its conformal nature, uniform compactness and thinner thickness. Mattelaer *et al.* reported the preparation of ultrathin amorphous Al_2O_3 coated $LiMn_2O_4$ by atomic layer deposition

[a]Key Laboratory of Material Physics, School of Physics and Engineering, Zhengzhou University, Zhengzhou 450052, P. R. China. E-mail: wxclhm@zzu.edu.cn

[b]Physics and Electronic Engineering Department, Xinxiang University, Xinxiang 453000, P. R. China. E-mail: zhanglw2004@126.com

[c]Jiangxi Jinhui Lithium Electric Materials CO. LTD, Fuzhou 336000, P. R. China

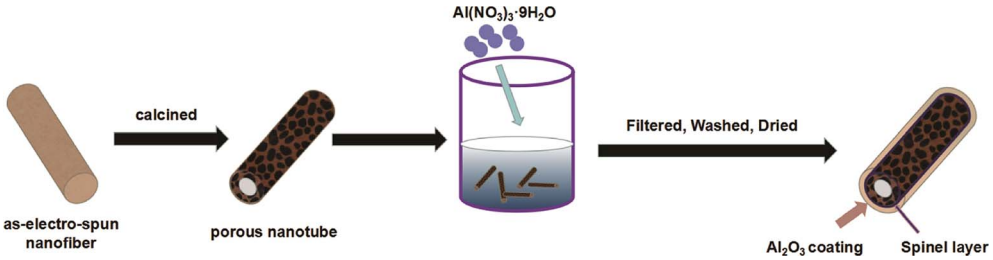

Fig. 1 Schematic diagram of the route used to synthesize Al_2O_3-coating Li-rich nanotubes.

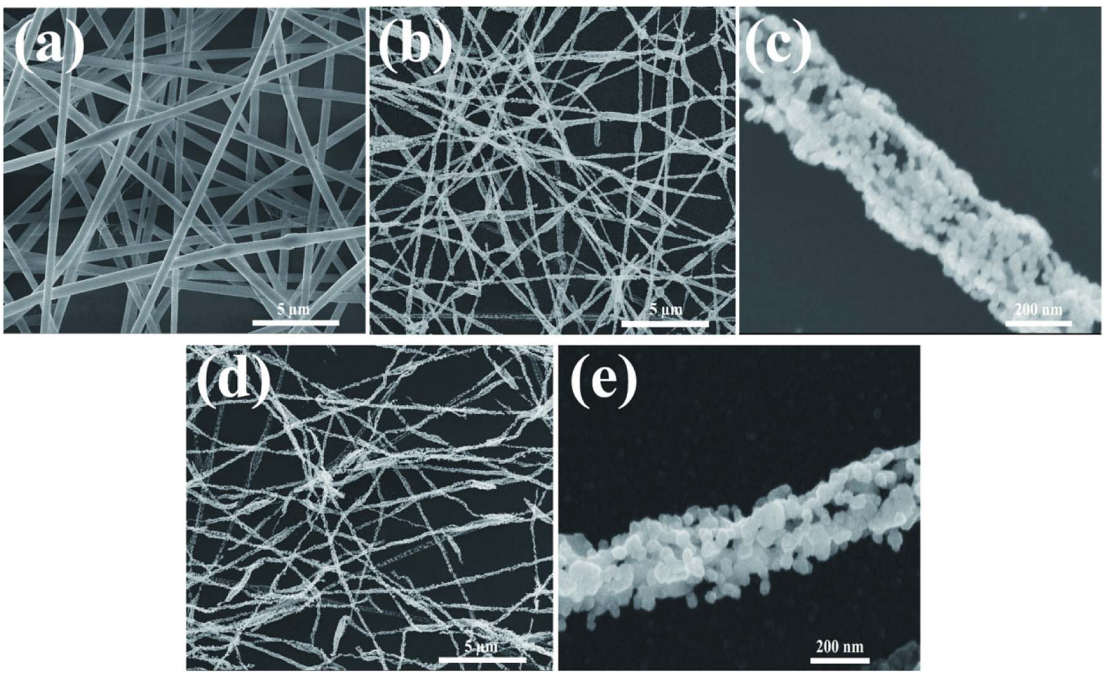

Fig. 2 SEM images of (a) as-electrospun LMNCO precursor nanofibers. (b and c) LMNCO nanotubes. (d and e) S-LMNCO nanotubes.

(ALD) method. The results showed that the surface coating materials exhibited improved rate capability.[22] Laskar *et al.* prepared MgO-coated $Li[Ni_{0.5}Mn_{0.3}Co_{0.2}]O_2$ (NMC) cathode by atomic layer deposition method. The results showed that cyclic performance was significantly improved.[23] However, all of these are studies on the coating of nanoparticles, and no research has been reported on the surface coating of one dimensional (1D) lithium-rich oxide.

In this paper, $Li_{1.2}Mn_{0.54}Ni_{0.13}Co_{0.13}O_2$ nanotubes were prepared by electrospinning method and surface modified by Al_2O_3. The effects of the coating amount of Al_2O_3 on the electrochemical performance of composites were studied in detail.

2. Experimental

2.1. Preparation of LMNCO nanotubes

Layered lithium-rich manganese oxide $Li_{1.2}Mn_{0.54}Co_{0.13}Ni_{0.13}O_2$ (LMNCO) nanotubes were synthesized by electrospinning method. Polyacrylonitrile (PAN, 1.5 g) was firstly added into 15 ml *N*,*N*-dimethylformamide (DMF) and stirred for 12 h at 60 °C. Then, a certain amount of $LiCH_3COO\cdot 2H_2O$, $Co(CH_3COO)_2\cdot 4H_2O$, $Ni(CH_3COO)_2\cdot 4H_2O$ and $Mn(CH_3COO)_2\cdot 4H_2O$ were added into the PAN/DMF solution under the constant stirring for 12 h at 60 °C to form a homogeneous electrospinning solution. The process of electrospinning was executed with a high voltage of 15 kV, 1 ml h^{-1} flowing rate and a distance of 200 mm between needle and collector. Subsequently, the as-electrospun nanofibers were collected on copper foil and calcined at 800 °C for 10 h in air atmosphere under a heating rate of 2 °C min^{-1} to obtain the LMNCO nanotubes.

2.2. Preparation of S-LMNCO nanotubes

As shown in Fig. 1, the LMNCO (5 g) was mixed into 300 ml deionized water, and $Al(NO_3)_3\cdot 9H_2O$ (2 g, 4 g, 6 g) was dissolved in the LMNCO suspension and stirred for 12 h, respectively. Then, the composites were dried by freeze drying technology after washing and filtering. At last, products were collected after drying at 500 °C for 10 h in the air, which were labeled as S-LMNCO-2, S-LMNCO-4, S-LMNCO-6.

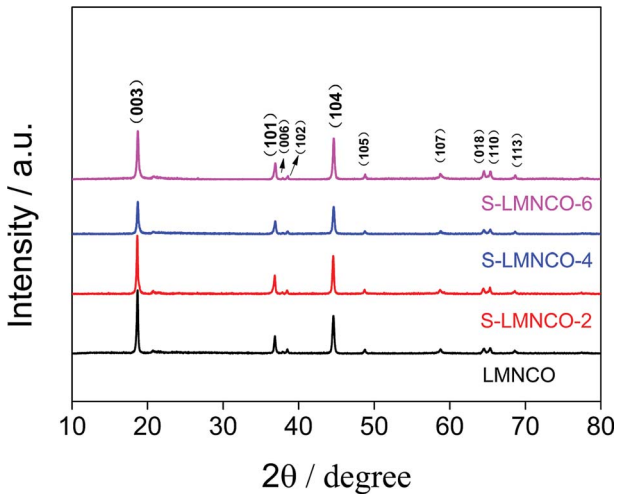

Fig. 3 The XRD patterns of LMNCO and S-LMNCO.

Table 1 Lattice parameters of the samples

Sample	a (Å)	c (Å)	c/a	$I_{(003)}/I_{(104)}$
LMNCO	2.8534	14.2186	4.9830	1.88
S-LMNCO-2	2.8543	14.2384	4.9884	1.84
S-LMNCO-4	2.8520	14.2166	4.9847	1.35
S-LMNCO-6	2.8520	14.2219	4.9867	1.26

2.3. Characterization

The microstructure and morphology of the nanotubes were examined by scanning electron microscopy (SEM) (JSM-6700F). The X-ray diffraction (XRD) patterns were collected on a Bruker D8 advanced diffractometer. The valence states of the metal elements were characterized by X-ray photoelectron spectroscopy (XPS, Thermo ESCALAB 250Xi). High-resolution transmission electron microscopy (HRTEM, JEOL JEM-2100F) with energy dispersive X-ray spectroscopy (EDS) were performed to examine the microstructure and elemental distribution of S-LMNCO-4 sample.

2.4. Electrochemical measurements

For the electrochemical measurements, a mass ratio of 8 : 1 : 1 of active material, PVDF and acetylene black, respectively, was used for the electrode fabrication. The wafer electrodes were punched for coin cells with the diameters of 1 cm and the coating capacity is about 3 mg cm^{-2}. The electrode was then stamped and placed in a vacuum oven for 24 h and finally assembled in a CR-2032 coin cell. The constant current charging and discharging measurements were performed on a battery test system (CT-4008, Neware) in the voltage range of 2.0–4.8 V. Cyclic voltammetry (CV) curves were measured at a scan rate of 0.1 mV on the electrochemical workstation (CHI750A). The electrochemical impedance spectroscopy (EIS) was tested with an amplitude of 5 mV and a frequency range from 0.01 Hz to 100 kHz on CHI750A electrochemical workstation.

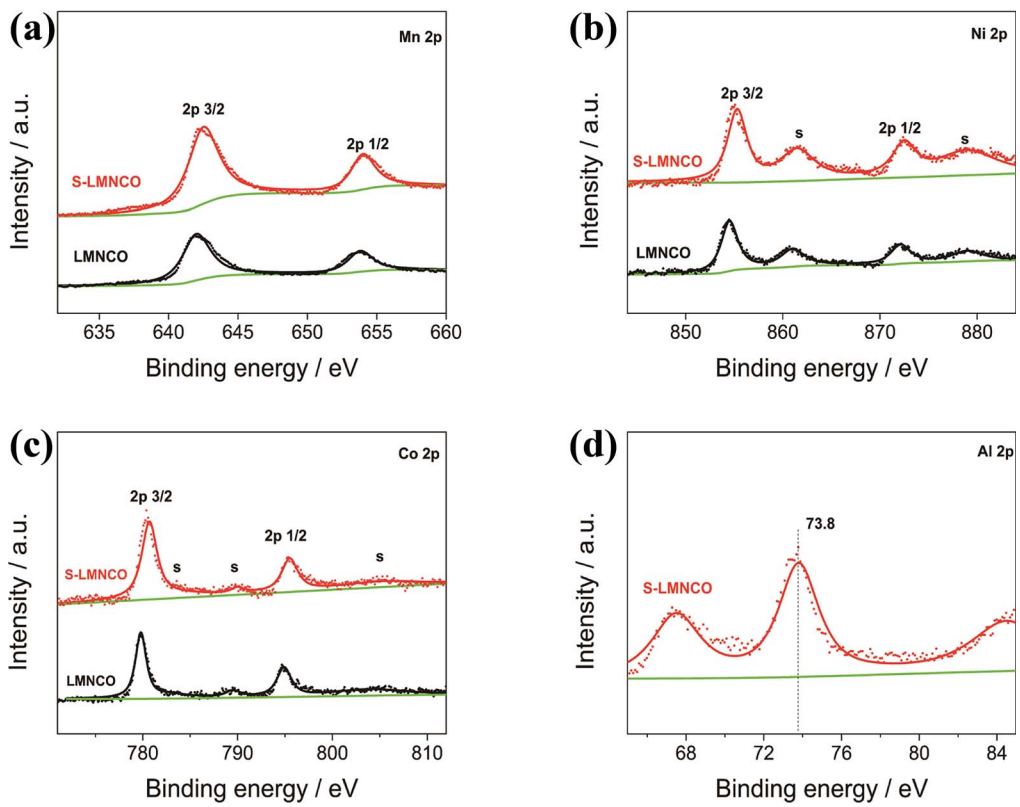

Fig. 4 XPS spectra of the (a) Mn 2p (b) Ni 2p (c) Co 2p (d) Al 2p of the LMNCO and S-LMNCO.

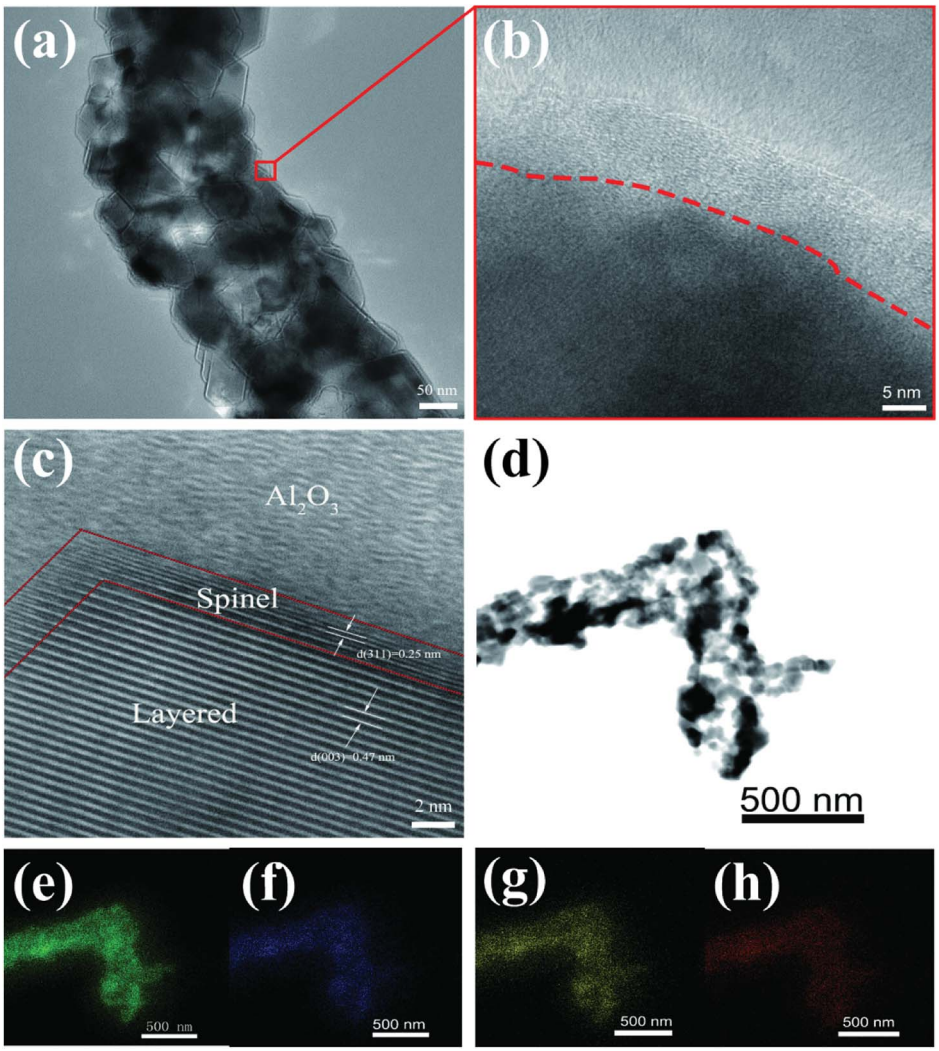

Fig. 5 (a) TEM images. (b and c) HRTEM images of S-LMNCO-4 sample. (d–h) EDS mapping of S-LMNCO-4 sample.

3. Results and discussion

3.1. Morphology and structure

As shown in Fig. 2, morphologies of the LMNCO nanotubes and surface-coating LMNCO nanotubes were examined by SEM. The as-electrospun LMNCO (Fig. 2a) precursor nanotubes exhibited a smooth surface with a length of hundreds micrometers and ~600 nm in diameters. As shown in Fig. 2b and c, owing to the decomposition of polymer (PAN) and acetate salts during calcination, the nanotubes exhibited a porous and hollow structure and reduced to 250 ± 50 nm in diameter. Furthermore, it can be seen that LMNCO nanotubes are composed of nanograins in the form of chains. It is noteworthy that there is no obvious change on the LMNCO nanotubes after $Al(NO_3)_3 \cdot 9H_2O$ surface modified in Fig. 2d and e, indicating that Al_2O_3 coating has little effect on the morphology of LMNCO.

Fig. 3 shows the XRD patterns of S-LMNCO (2, 4, 6) and LMNCO samples. All samples have a hexagonal α-$NaFeO_2$ structure with space group *R*3*m*. The broad peak around 20–23° is attributed to the monoclinic Li_2MnO_3 phase (*C*2/*m*).[1,16] In addition, clearly splitting of (006)/(102) peaks and (018)/(110) peaks of all samples suggesting the lattice of composites have a well-defined layered structure.[18] Lattice constants are summarized in Table 1. There is no apparent variation in parameters *a* and *c* for the before and after surface modified samples. Moreover, the intensity ratio of the (003) and (104) peaks is relevant to the cationic mixing degree.[24] With increasing Al_2O_3 content, the value of $I_{(003)}/I_{(104)}$ decreased from 1.88 to 1.26, but the value of $I_{(003)}/I_{(104)}$ for all samples are greater than 1.2, which indicates both materials suppressed cation mixing.

To investigate the valence of the transition-metal ions of LMNCO and S-LMNCO, XPS measurements were conducted for these two cathode materials in Fig. 4. The Mn $2p_{3/2}$, Ni $2p_{3/2}$ and Co $2p_{3/2}$ peaks of two samples are located at 642.5 eV, 780.8 eV and 855.1 eV, indicating that the chemical valences of Mn, Co and Ni are +4, +3 and +2, respectively.[24,25] Additionally, a peak appearing around 73.8 eV (Fig. 4d) can only be observed in S-LMNCO sample, which is corresponding to the Al $2p_{3/2}$ BE obtained in Al_2O_3.[18] We will demonstrate that Al_2O_3 is successfully coated on the surface of LMNCO nanotubes in following discussions.

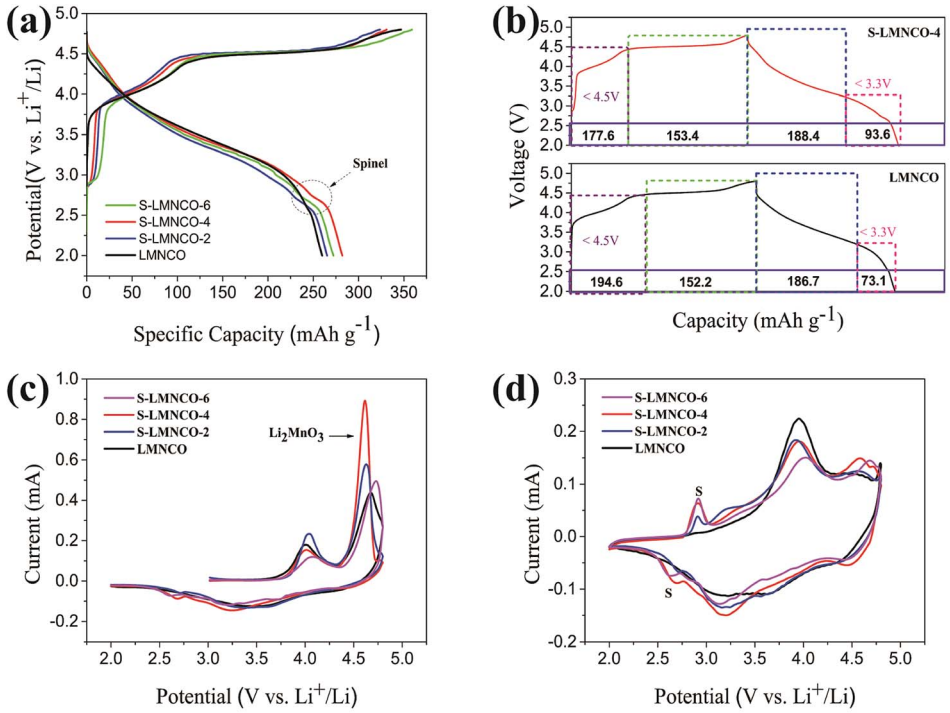

Fig. 6 (a) The initial charge–discharge curves. (b) Quantitative correlation of the first cycling curves of S-LMNCO-4 and LMNCO cells. (c and d) CV of the first cycle and second cycle.

Fig. 5 shows TEM and HRTEM images of S-LMNCO-4 sample. As shown in Fig. 5b, there is an amorphous layer of 7–10 nm thickness covering on the material surface. In Fig. 5c, the lattice spacing of 0.47 nm corresponds to the spacing between (003) planes of the layered LMNCO structure. Moreover, it is noteworthy that there is a coexistence of the spinel layer with a thickness of about 2 nm between LMNCO layered structure and Al_2O_3 coating. The lattice spacing of 0.25 nm is well indexed to the (311) plane of cubic spinel structures.[26] Spinel structure on the surface of material can provide three-dimensional diffusion paths, which can effectively improve the lithium ions and electrons diffusivity.[27] Thus the appearance of the spinel layer will be beneficial to the improvement of the electrochemical performances of LMNCO. The EDS mapping of S-LMNCO-4 sample is shown in Fig. 5e–h, and the results show that the distribution of Al, Mn, Ni and Co elements is consistent,[15,18] indicating that the Al_2O_3 film is uniformly coated on the surface of the LMNCO nanotubes and the LMNCO@Al_2O_3 core–shell structure is formed.

3.2. Electrochemical performance

The initial charge–discharge curves of all the samples between 2.0 V and 4.8 V at a current density of 25 mA g^{-1} are shown in Fig. 6a and Table 2. The LMNCO sample exhibits a signature curve of lithium-rich cathode material. The Li^+ ion de-intercalation from the LMNCO component corresponding the sloping curve below 4.5 V, the "Li_2O" extraction from the Li_2MnO_3 phase relating to plateau around 4.5 V.[7,28] Obviously, the curve shape of the S-LMNCO samples show a significant difference from the pristine sample at the beginning of charge and the end of discharge cycle, the CV clearly illustrates that the spinel phase appears at around 2.7 V in Fig. 6b. In addition, S-LMNCO electrodes exhibited better coulombic efficiency and discharge capacity, especially for the S-LMNCO-4 sample, which exhibited an initial coulombic efficiency of ~85.2% and a specific discharge capacity of ~282.04 mA h g^{-1}. While for the LMNCO electrode, the discharge capacity and initial coulombic efficiency were only ~259.74 mA h g^{-1} and ~74.9%, respectively, the detailed information is listed in Table 2. It demonstrated that a suitable amount of spinel phases produced contribute to the promotion of electrochemical properties.[29,30] Moreover, we perform a quantitative analysis of the charge and discharge capacity of LMNCO sample and S-LMNCO-4 sample to estimate the capacity contributed by the spinel phase (Fig. 6b). There are two apparent differences throughout the charge and discharge process. Firstly, the charging capacity of the LMNCO cell is larger than that of the S-LMNCO-4 cell when the charging voltage is less than 4.5 V, indicating that the transition-metal oxidation in LMNCO sample is more than S-LMNCO-4 sample. Secondly, the S-LMNCO-4 sample has

Table 2 The initial charge–discharge capacities and efficiencies of LMNCO and S-LMNCO

Sample	Charging (mA h g^{-1})	Discharging (mA h g^{-1})	Efficiency (%)
LMNCO	346.83	259.74	74.9
S-LMNCO-2	323.67	265.22	81.9
S-LMNCO-4	330.98	282.04	85.2
S-LMNCO-6	358.95	272.23	75.8

a higher discharge capacity than LMNCO sample (20.5 mA h g^{-1}) below 3.3 V. During the potential from 3.3 to 2.0 V, the discharge capacity is primarily provided by the reduction of Mn^{4+}/Mn^{3+}.[31,32] Therefore, the presence of spinel phase is an essential factor in the improvement of S-LMNCO cell.

In order to investigate the redox reaction of LMNCO sample and S-LMNCO sample during the charging and discharging, cyclic voltammograms (CVs) have been performed to probe between 2.0 V and 4.8 V at a sweep rate of 0.1 mV s^{-1} in Fig. 6c and d. There are two main oxidation peaks appearing at 4.0 V and 4.6 V during the first charging (Fig. 6c). The oxidation peak around 4.0 V is relevant to the oxidation of Ni^{2+} to Ni^{4+} and Co^{2+} to $Co^{3.6+}$, and another oxidation peak around 4.6 V owing to removal of oxygen from Li_2MnO_3 component and further oxidation of $Co^{3.6+}$ to Co^{4+}.[33,34] Obviously, the S-LMNCO-4 sample has a higher peak at 4.6 V, suggesting a higher Li^+ transfer rate between Li_2MnO_3 and layered component. The disappearance of oxidation peak at 4.6 V in the second cycle indicates the activation of the Li_2MnO_3 is suppressed and the loss of oxygen from Li_2MnO_3 is irreversible.[35,36] In addition, in Fig. 6c, we find the appearance of a spinel peak at 2.7 V, which corresponds well to the previous CE curve (Fig. 6a).

The cyclic performances of the LMNCO and S-LMNCO (2, 4, 6) at 1C (250 mA h g^{-1}) are shown in Fig. 7a. Obviously, surface-modification samples show better discharge cycling performance than LMNCO sample. The discharge capacity of LMNCO sample fades to 112 mA h g^{-1} after 90 cycles, and its capacity retention is 78.3%. In all samples of S-LMNCO (2, 4, 6), the discharge capacity of S-LMNCO-4 retained 97.6% (210 to 205 mA h g^{-1}), exhibited the best cyclic stability. In addition, compared with the Al_2O_3 coated LMNCO nanoparticles which was Zhou's work (about 78.9%),[21] there was an obvious improvement.

Fig. 7b shows the rate of capacity of LMNCO and S-LMNCO samples at rates of 0.1, 0.2, 0.5, 1, 2, 5 and 0.1C. Comparison to the pristine LMNCO cathode, the surface-coated nanotubes displayed improved rate capability, and especially at the high current density. Moreover, it can be apparently observed in Fig. 7c and d that the ΔV value of S-LMNCO sample is less than LMNCO sample, which illustrates S-LMNCO sample has much low polarization.[31,37] Excellent rate performance thanks to the excellent structural design of the material, where one-dimensional (1D) nanostructures can enhance the Li^+ diffusion coefficient and electronic conductivity.[38] Furthermore, the spinel phase on the interface has a 3D Li^+ diffusion channel, which can provide a faster Li diffusion rate.[39] Compared with the literature,[15,16] it can be found that the diameter and the calcination temperature have significant effects on the electrochemical properties of the nanotubes, and the large inner diameter and the high calcination temperature are benefit to improve the electrochemical properties of the nanotubes. The inner diameter and calcination temperature of our sample are smaller than that of ref. 15 and similar to ref. 16. Therefore, the electrochemical performance of our pristine sample is worse than that of ref. 15, but obviously superior to that of ref. 16. However, the results show that the electrochemical properties of our samples coated with Al_2O_3 are superior to those of ref. 15 and 16.

In order to further understand the superior electrochemical performance of S-LMNCO electrode, the electrochemical

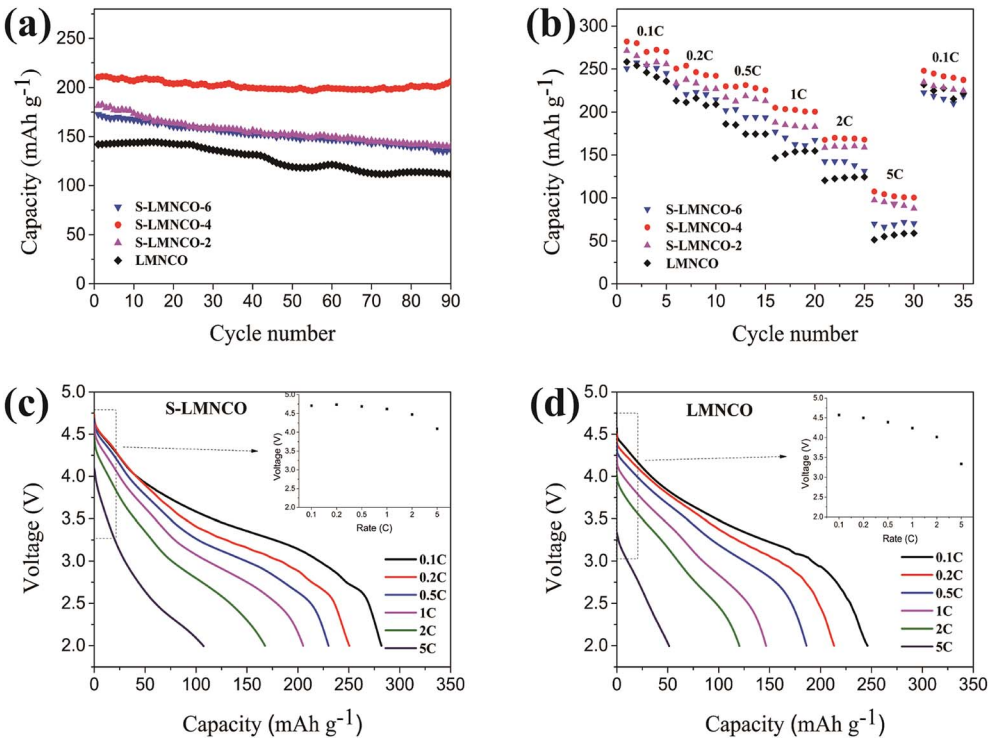

Fig. 7 (a) Cyclic stability performance. (b) Rate capacity of LMNCO and S-LMNCO. Discharge profiles for the (c) LMNCO and (d) S-LMNCO.

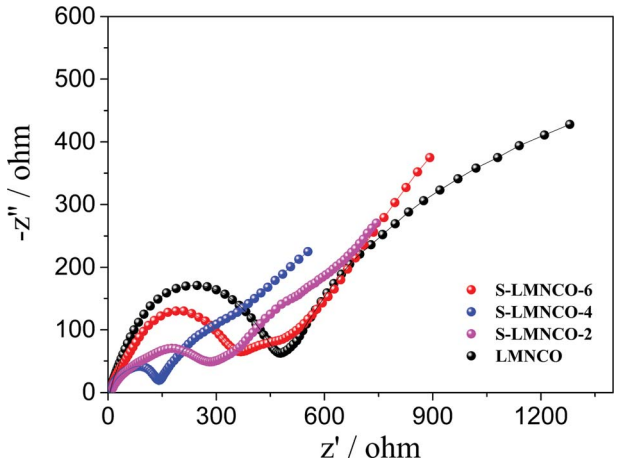

Fig. 8 The Nyquist plots of sample LMNCO, S-LMNCO-2, S-LMNCO-4 and S-LMNCO-6.

impedance spectroscopy (EIS) of sample LMNCO and S-LMNCO (2, 4, 6) are given in Fig. 8. The Nyquist plots of all samples consist of two parts: semicircle and a slope. The first part, semicircle in high frequency region, corresponds to the process of charge transfer though the electrolyte/electrode interface, and the diameter of semicircle represent the charge transfer resistance (R_{ct}).[40] The second part, slope in the low frequency region, relates to the solid-state lithium ion diffusion process in the active materials. It can be obviously seen from the figure that S-LMNCO-4 sample has a smaller semicircle diameter than other samples, indicating the smallest charge transfer resistance at the interface.

4. Conclusions

In summary, Al_2O_3 surface-coated LMNCO nanotubes have been synthesized by electrospinning followed by surface coating, and the TEM measurement confirmed that the spinel phase is formed in the interface between LMNCO and Al_2O_3 coating. After surface modified, the S-LMNCO nanotubes exhibited excellent electrochemical performance than pure LMNCO nanotubes. On the one hand, Al_2O_3 coating can stabilize the interface between electrolyte and electrode materials, the capacity retention increased from 78.3% to 97.6% after 90 cycles. On the other hand, the built-in spinel tunnels caused by the coating process provide an efficient Li^+ diffusion channel, which is beneficial to reduce irreversible capacity loss in the initial cycle (282.04 mA h g^{-1}, 85.2%) and promote the rate capability. With outstanding electrochemical performance, we believe that this new design strategy will contribute to development of next generation rechargeable lithium-ion batteries.

Conflicts of interest

There are no conflicts to declare.

Acknowledgements

The authors gratefully acknowledge the financial support of the National Natural Science Foundation of China (No. 51802288), the China Postdoctoral Science Foundation (No. 2017M622369) and the Key Projects of Higher Education in Henan Province (No. 18A140008).

References

1 S. Kim, W. Cho, X. Zhang, Y. Oshima and J. W. Choi, *Nat. Commun.*, 2016, **7**, 13598.
2 H. Meng, X. Pang and Z. Zhen, *J. Power Sources*, 2013, **237**, 229–242.
3 Q. Li, G. Li, C. Fu, D. Luo, J. Fan and L. Li, *ACS Appl. Mater. Interfaces*, 2014, **6**, 10330.
4 J. Xu, M. Sun, R. Qiao, S. E. Renfrew, L. Ma, T. Wu, S. Hwang, D. Nordlund, D. Su and K. Amine, *Nat. Commun.*, 2018, **9**, 947.
5 B. Song, H. Liu, Z. Liu, P. Xiao, M. O. Lai and L. Lu, *Sci. Rep.*, 2013, **3**, 3094.
6 Z. H. Guan, Y. Wang, G. Chen and H. O. Wang, *J. Cheminf.*, 2010, **37**, 17479–17487.
7 Y. Pei, C. Y. Xu, Y. C. Xiao, Q. Chen, B. Huang, B. Li, S. Li, L. Zhen and G. Cao, *Adv. Funct. Mater.*, 2017, **27**, 1604349.
8 M. M. Thackeray, S. H. Kang, C. S. Johnson, J. T. Vaughey and S. A. Hackney, *Electrochem. Commun.*, 2006, **8**, 1531–1538.
9 T. A. Arunkumar, Y. Wu and A. Manthiram, *Chem. Mater.*, 2007, **19**, 3067–3073.
10 N. Li, Y. S. He, X. Wang, W. Zhang, Z. F. Ma and D. Zhang, *Electrochim. Acta*, 2017, **231**, 363–370.
11 J. Yao, X. Wang, X. Zhao, J. Wang, H. Zhang, W. Yu, G. Liu and X. Dong, *Electron. Mater. Lett.*, 2016, **12**, 1–8.
12 A. R. Armstrong, M. Holzapfel, P. Novak, C. S. Johnson, S. H. Kang, M. M. Thackeray and P. G. Bruce, *J. Am. Chem. Soc.*, 2006, **128**, 8694.
13 L. Liu, C. Lu, M. Xiang, Y. Zhang, H. Liu and H. Wu, *ChemElectroChem*, 2017, **4**, 332–339.
14 G. Xu, J. Li, X. Li, H. Zhou, X. Ding, X. Wang and F. Kang, *Electrochim. Acta*, 2015, **173**, 672–679.
15 D. Ma, Y. Li, P. Zhang, A. J. Cooper, A. M. Abdelkader, X. Ren and L. Deng, *J. Power Sources*, 2016, **311**, 35–41.
16 L. L. Cui, X. W. Miao, Y. F. Song, W. Y. Fang, H. B. Zhao and J. Hui, *Adv. Manuf.*, 2016, **4**, 79–88.
17 B. Xiao, B. Wang, J. Liu, K. Kaliyappan, Q. Sun, Y. Liu, G. Dadheech, M. P. Balogh, L. Yang and T. K. Sham, *Nano Energy*, 2017, **34**, 120–130.
18 X. Wen, K. Liang, L. Tian, K. Shi and J. Zheng, *Electrochim. Acta*, 2017, **260**, 549–556.
19 D. Ma, Y. Li, M. Wu, L. Deng, X. Ren and P. Zhang, *Acta Mater.*, 2016, **112**, 11–19.
20 M. R. Laskar, D. H. Jackson, S. Xu, R. J. Hamers, D. Morgan and T. F. Kuech, *ACS Appl. Mater. Interfaces*, 2017, **9**, 11231–11239.
21 C. X. Zhou, P. B. Wang, B. Zhang, J. C. Zheng, Y. Y. Zhou, C. H. Huang and X. M. Xi, *J. Electrochem. Soc.*, 2018, **165**, A1648–A1655.

22 F. Mattelaer, P. M. Vereecken, J. Dendooven and C. Detavernier, *Adv. Mater. Interfaces*, 2017, **4**, 1601237.
23 M. R. Laskar, D. H. Jackson, S. Xu, R. J. Hamers, D. Morgan and T. F. Kuech, *ACS Appl. Mater. Interfaces*, 2017, **9**, 11231–11239.
24 R. Yu, Z. Zhang, S. Jamil, J. Chen, X. Zhang, X. Wang, Z. Yang, H. Shu and X. Yang, *ACS Appl. Mater. Interfaces*, 2018, **10**, 10561–16571.
25 W. K. Pang, H. F. Lin, V. K. Peterson, C. Z. Lu, C. E. Liu, S. C. Liao and J. M. Chen, *Chem. Mater.*, 2017, **29**, 10299–10311.
26 C. Yang, S. Han, J. Huang and M. Qian, *Mater. Chem. Phys.*, 2015, **149–150**, 695–700.
27 W. Xu and Y. Wang, *Ionics*, 2017, **24**, 1–10.
28 Y. Jin, Y. Xu, X. Sun, L. Xiong and S. Mao, *Appl. Surf. Sci.*, 2016, **384**, 125–134.
29 J. Lee, D. A. Kitchaev and D. H. Kwon, *Nat. Commun.*, 2018, **8**, 185–190.
30 Q. Liu, X. Su, D. Lei, Y. Qin, J. Wen, F. Guo, Y. A. Wu, Y. Rong, R. Kou and X. Xiao, *Nat. Energy*, 2018, **1**, 8.
31 R. Yu, X. Zhang, T. Liu, L. Yang, L. Liu, Y. Wang, X. Wang, H. Shu and X. Yang, *ACS Appl. Mater. Interfaces*, 2017, **9**, 41210–41223.
32 X. Feng, Y. Gao, L. Ben, Z. Yang, Z. Wang and L. Chen, *J. Power Sources*, 2016, **317**, 74–80.
33 R. Yu, G. Wang, M. Liu, X. Zhang, X. Wang, H. Shu, X. Yang and W. Huang, *J. Power Sources*, 2016, **335**, 65–75.
34 I. Kim, J. Knight, H. Celio and A. Manthiram, *J. Mater. Chem. A*, 2014, **2**, 8696–8704.
35 D. Mohanty, S. Kalnaus, R. A. Meisner, K. J. Rhodes, J. Li and E. A. Payzant, *J. Power Sources*, 2013, **229**, 239–248.
36 Z. He, Z. Wang, H. Chen, Z. Huang, X. Li, H. Guo and R. Wang, *J. Power Sources*, 2015, **299**, 334–341.
37 C. Yang, X. Zhang, J. Huang, P. Ao and G. Zhang, *Electrochim. Acta*, 2016, **196**, 261–269.
38 K. Zhang, X. Han, Z. Hu, X. Zhang, Z. Tao and J. Chen, *J. Cheminf.*, 2015, **46**, 699–728.
39 V. N. Hung, P. Arunkumar and I. W. Bin, *Sci. Rep.*, 2017, **7**, 45579.
40 L. He, J. Xu, T. Han, H. Han, Y. Wang and J. Yang, *Ceram. Int.*, 2017, **43**, 5267–5728.